Macromolecules **2001,** *34,* 2710−2718

Interfacial Fracture between Highly Cross-Linked Polymer Networks and a Solid Surface: Effect of Interfacial Bond Density

Mark J. Stevens

Sandia National Laboratories, MS 1111, P.O. Box 5800, Albuquerque, New Mexico 87185-1111

Received March 28, 2000; Revised Manuscript Received February 13, 2001

ABSTRACT: For highly cross-linked polymer networks bonded to a solid surface, the effect of interfacial bond density and system size on interfacial fracture is studied using molecular dynamics simulations. Results for tensile and shear mode simulations are given. The correspondence between the stress−strain curve and the sequence of molecular deformations is obtained. The failure strain for a fully bonded surface is equal to the strain necessary to make taut the average of the minimal paths through the network from a bonded site on the bottom solid surface to a bonded site on the top surface. At fractional interfacial bond densities, cavities form above the nonbonded surface, yielding an inhomogeneous strain profile and a smaller failure strain. The failure strain and stress are linearly proportional to the number of bonds at the interface except in the tensile mode when number of bonds is so few that van der Waals interactions dominate. The failure mode is successfully constructed to be interfacial by limiting the interfacial bond density to be less than the bulk bond density.

I. Introduction

Adhesives present a complex problem for polymer theory. Progress has primarily occurred for adhesives with weak interfacial strength[1] such as pressure-sensitive adhesives[2] and polymer−polymer interfaces.[3] Such adhesives typically do not have strong chemical bonds across the interface. Only relatively weak van der Waals interactions exist at these interfaces. For strong adhesives equivalent development is lacking. The nature of the interface between the adhesive and a rigid adherend is especially important as this region tends to be the weak link. Fracture mechanics methods have used to analyze the interfacial failure in such systems.[5] A more robust theory requires additional knowledge about the physical phenomena occurring at the interface distinct from the bulk. The difficulty of measuring properties of interfaces has been a major obstacle in understanding interfacial adhesion issues. Recent experiments at Sandia have begun to study failure for the strong interface formed between an epoxy and a silicon wafer.[4,6] The interfacial structure is probed with neutron and X-ray reflectivity. In addition, the number of chemical bonds at the interface is varied in a controlled manner through the use of self-assembled monolayer (SAM) coatings.[7] In conjunction with these experiments, a program of molecular dynamics (MD) simulations has been developed. The initial results of these MD simulations are reported here.

In bulk epoxies, experiments have shown that as the cross-link density increases, the bulk failure mechanism changes from crazes to deformation zones.[8] The bond strength is strongest in the highly cross-linked limit. Only this highly cross-linked regime is treated in this work. There is very little information about mechanisms for interfacial failure in epoxies on solid surfaces. Linear elastic fracture mechanics works well for such polymers in the limit of small scale yielding.[9] The large stresses near the crack tip can be treated in terms of the stress intensity factor, K. However, this is a phenomenological approach in which K is not calculated from material properties but calculated from measured quantities. Performing MD simulations that treat the region near the crack tip would yield very useful, but, thus far, missing, information. Ultimately, we would like to be able to use such information to either calculate quantites such as K or directly determine the stress field near the crack tip.

From a general perspective, the polymer adhesive is a network. We would like to know how the network structure influences the adhesive strength, the initiation of cracks, the distribution of stress, etc. In a random network, there will be a distribution of stress on the bonds, and the network bonds that are most stressed will break first.[10] Crack initiation could occur where a cluster of highly constrained bonds exists. There is no a priori reason to expect the crack initiation site to occur at the interface, although we know experimentally that interfaces are often weak.

Little work exists for molecular simulation of polymer adhesives.[11] Highly cross-linked polymer networks have been particularly neglected in simulation work, yet they are important class of adhesives. The development of MD simulations has reached the point where treatment of adhesives is possible.[11] Simple coarse-grained bead−spring models successfully treat bulk polymer melts and networks.[12,13] The present work extends these methods to study interfacial fracture of highly cross-linked polymer networks. Connectivity is the main ingredient in polymer dynamics.[14] Bead−spring models maintain connectivity by not allowing polymer strands to cross without bond breaking. A bead represents a group of monomers; the number depends on the particular polymer. Typically, the stiffer the polymer, the more monomers per bead. Any simulation is limited in the time scales that computational resources allow. The coarse graining allows the simulations to reach times of at least a microsecond. This enables coarse-grained MD simulations to treat entanglement dynamics.[15] In contrast, atomistic simulations can barely pass a nanosecond.

To understand how varying interfacial bonding affects interfacial strength, the number of chemical bonds between the adhesive and the solid surface is varied. The stress−strain curves are then calculated as a

10.1021/ma000553u CCC: $20.00

function the number of interfacial bonds using MD. The structural dynamics is examined and correlated with the stress−strain curves.

In the following section, the bead−spring model is described along with other aspects of the simulations. The results of the simulations are presented in section III. The correspondence between the stress−strain curve and the sequence of molecular deformations is given. The relationship between the structure and the failure strain is described. Insights based on force measurements between self-assembled monolayers reveal the expected range of stress magnitudes for chemical and physical interactions. Next, the stress−strain curves are presented as a function of the number of interfacial bonds. In section IV, the results are discussed. The inhomogeneity in the strain is demonstrated and shown to be an additional constraint on the network affecting the failure strain. Finally, the conclusions are summarized in section V.

II. Simulation Method

A. Polymer Model and Potentials. The polymer network is treated as a bead−spring system. Beads interact via a Lennard-Jones (LJ) potential with a cutoff at $2.5d$.[13]

$$U_{\mathrm{LJ}}(r) = 4u_0\left[\left(\frac{d}{r}\right)^{12} - \left(\frac{d}{r}\right)^{6}\right] \tag{1}$$

In this article d represents the LJ diameter and u_0 represents the LJ energy. The traditional notation of σ and ϵ for stress and strain, respectively, is used. All quantities will be in LJ units.

The LJ stress will later be mapped to engineering units. Because of the coarse-grained nature, there is no one-to-one mapping of the model system to the actual system. In coarse-grained simulations, the goal is to understand the model system self-consistently. In relating the simulation results to actual adhesives such as epoxies, the emphasis is on the connectivity and its implications.

In the Kremer−Grest model,[13] beads are bonded together using a potential that prevents chain crossing. This bond potential is the sum of the purely repulsive LJ interaction with a cutoff at $2^{1/6}d$ and a finite-extensible nonlinear elastic (FENE) attractive potential. To allow bond breakage and preserve the continuity of the bond force, a quartic bond potential was created to replace the FENE potential.

$$\begin{aligned} U_4(r) &= k_4(y - b_1)(y - b_2)y^2 + U_0, \quad r < r_c \\ &= U_0, \quad r \geq r_c \end{aligned} \tag{2}$$

where $y = r - \Delta r$ shifts the quartic center from the origin. The value of b_1 is set to match the FENE bond minimum. The potential is smoothly cutoff at r_c. Once a bond separation is larger than r_c, the bond is broken and the bond potential between the pair turned off, preventing the bond from re-forming. The potential parameters are $k_4 = 1434.3u_0/d^4$, $b_1 = -0.7589d$, $b_2 = 0.0$, $\Delta r = 1.5d$, $r_c = 1.5d$, and $U_0 = 67.2234u_0$. The parameters were determined by fitting the total bond force with the quartic component to the bond force with the FENE component at the first zero and the minimum. This just leaves the maximum bond force as a free variable.

The maximum bond force is $156.7\ u_0/d$, and the maximum LJ force is $2.4\ u_0/d$. For atomic force fields, the force ratio between a covalent bond and the van der Waals forces is about 1000. However, in the simulations a single bead represents several atoms, and the LJ pair interaction represents multiple van der Waals pair interactions. With even just three atoms per bead, each bead−bead interaction represents nine pair interactions. Thus, the force ratio of 65 used in these simulations is in the correct range.

B. Solid Surface Model. The complete system consists of a polymer network between two solid walls. Each wall is composed of two layers of particles in an fcc lattice with nearest-neighbor distance $1.204d$. The (111) direction (z-direction) is perpendicular to the walls. The wall particles are bound to the lattice sites by a harmonic spring with spring constant $100u_0/d^2$. The wall dimensions give the simulation cell lateral lengths, L_x and L_y, and periodic boundary conditions are applied in these directions. The separation distance between the innermost wall layers is L_z. The wall particles interact with the beads via the same LJ potential in eq 1. Some wall particles bond to the polymer network by eq 2 as will be described in the next section. To perform the tensile pull and shear simulations, the walls are pulled at constant velocity.

C. Network Formation. To form the networks, we take a cue from a highly cross-linked adhesive, epoxies. Epoxies are chemically cured networks formed from a liquid mixture of a resin (e.g., Bisphenol A) and a cross-linker.[16] Each strand between cross-links consists of only a few monomers. As a bead corresponds typically to 2 or 3 monomers,[13] an epoxy model will have only a few beads per strand. The minimal case of two beads is used here. In this initial work the emphasis is on understanding general features of highly cross-linked networks. In later work, the simple modifications that would more precisely model specific epoxies will be applied. A discussion of possible modifications is given in section IV.C.

In epoxies, a liquid mixture of a cross-linker and a resin is cross-linked dynamically. In the simulations, a mixture consisting of two bead and three bead molecules is dynamically cross-linked. The three bead molecule has a 6-fold functional cross-linker bead already bonded to a two-bead strand. In this initial work, the strand beads and cross-linker beads have identical LJ parameters. The liquid is equilibrated at temperature $T = 1.1u_0$. The network is dynamically formed during a constant temperature simulation. Bonds are formed when the separation between a cross-linker and a strand end or wall particle is less than $1.3d$. After equilibrating the liquid mixture, cross-linkers are first bonded to the walls. Only a single bond to the wall per cross-linker is allowed. This is intended to promote interfacial failure over adhesive failure. Next, the cross-linkers are bonded to strands until at least 95% of all possible bonds are made. Zero load is maintained on the walls during the cross-linking. Afterward, the temperature is reduced below the glass transition temperature ($T_g = 0.5u_0$) to $0.3u_0$.

D. System Parameters. Four different system sizes have been studied. In general, one always wants to know the size scaling of simulation results. In adhesion problem, issues of size dependence are potentially even more important. Typically in molecular simulations, the simulation cell must only be large enough to encompass

Table 1. System Parameters

no.	no. of particles	area	height
1	14 000	$A_1 = 643$	15.1
2	51 500	$3A_1 = 1928$	19.9
3	91 000	1928	39.2
4	170 000	1928	77.0

the relevant molecular structure. In adhesion problems, larger scale structures exist. For example, estimates of the plastic zone size about a crack tip in an epoxy give values of about 10 μm, which is much larger than any possible simulation. Thus, the simulations need to be as large as possible, and while phenomena on a scale larger than the simulation cell cannot be directly treated, a set of a data for different sizes indicates the trends. Table 1 lists the varying size parameters for these systems. For system 1 the wall dimensions are $L_x = 33.1d$ and $L_y = 19.3d$. For systems 2–4, L_x is doubled and $L_y = 28.9d$. Given the size of epoxy constituent molecules, the bead size corresponds to about $d \simeq 1$ nm. Using this mapping, the largest system studied has a height of 77 nm. The simulations effectively treat the region at or near the crack tip. In this region, strains and possibly stresses are much larger than the macroscopic measured values.

The dynamics is performed at constant temperature T using the Langevin thermostat.[17] The Langevin equations of motion with random noise term **W** are

$$m\ddot{\mathbf{r}}_i = \mathbf{F}_i - m\Gamma\dot{\mathbf{r}}_i + \mathbf{W}_i(t) \tag{3}$$

where $\mathbf{r}_i$ and $\mathbf{F}_i$ are the ith particle's position and force, respectively, and Γ is the damping constant such that

$$\langle \mathbf{W}_i(t)\, \mathbf{W}_j(t')\rangle = 6k_{\mathrm{B}}Tm\Gamma\delta_{ij}\delta(t - t') \tag{4}$$

where m is the bead mass. The two additional terms to Newton's equation couple the system to a heat bath maintaining a constant, average temperature.

The integration time step is 0.005 τ, and the damping constants are 1 τ^{-1} for the monomers and 5 τ^{-1} for the walls, where τ is the LJ time unit.

Simulations of both tensile and shear deformations are performed. In both cases, the walls are moved at constant velocity. All the data presented here are for a wall velocity of $v = 0.01d/\tau$. Simulations have been performed for $v = 0.001d/\tau$ and 0.1 d/τ with similar results. For the shear simulations, the wall is pulled in the x-direction.

III. Results

A. Molecular Scale Deformation of Network. Figure 1 shows a typical tensile stress–strain curve. The correspondence between the molecular deformations and the stress–strain curve is as follows. The first peak at $\epsilon_y = 0.1$ is the yield stress. There is a maximum in the LJ force to separate neighboring pairs of beads. In equilibrium, the typical separation is 1d, and the maximum force is at $r = 2^{1/6}d = 1.12d$. Thus, it takes a strain of about 0.1 to reach the maximum value.

Beyond the small strain region, the stress is constant for a range of strains. In this plateau regime, examination of configurations shows that the bonds are not stretched. Instead, the strands connecting two cross-linkers are pulled progressively taut. In this section, "strand" includes the cross-linkers so that there are four beads to a strand. Only after the strands are in the taut, linear conformation do the bonds begin to stretch. Even though there are only four beads per strand, the strain to extend the strand from the compact initial state to the linear state is relatively large. For example, consider the close packed, planar state with the strand making a zigzag path from one cross-linker to the other. The bond length is about equal to d, and in the compact state the nonbonded beads are separated by the core diameter, d. In the linear, taut conformation the separation is 3d. The strain to deform the compact state into the linear state is 2. The plateau regime in Figure 1 has a range of strain of about 0.35. Clearly, the average strand conformation is not in the close packed state at $\epsilon = 0$, but also it is clear that large strains are possible even for short strands.

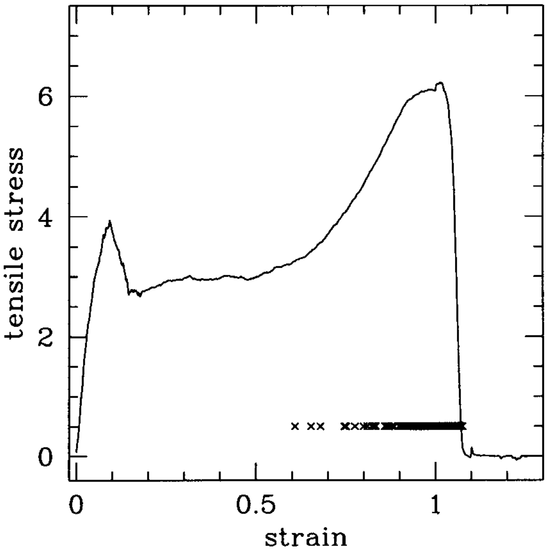

Figure 1. Tensile stress–strain curve for the fully bonded case of system 2. The points mark the strains at which bond breaking occurs. Stress is in LJ units.

Once strands are taut, bonds must stretch on further displacement. At this point, the stress rises. The points in Figure 1 show the strains at which bonds break. The first bond breaking occurs at $\epsilon = 0.60$. As more bonds are stretched, the stress rises and additional bonds break. Finally, the system fails at $\epsilon_f = 1.05$, where the failure strain is taken as the strain at the midpoint between the failure stress (peak) and zero stress. Failure is interfacial with all the bonds between the bottom surface and the network breaking.

In all the simulations failure occurs interfacially. The reason for this is that the areal bond density is lower at the interface than at any plane in the bulk. The cross-linkers bonded to the bottom surface have only a single bond in the $-z$ direction. Cross-linkers not at the interface have on average three bonds in the $+z$ direction and $-z$ direction. Thus, the interfacial cross-linker bonds have to support more load; consequently, they stretch and break first.

B. Minimal Paths. To understand the failure strains in terms of the network structure, first consider the maximum strain possible without bonds breaking. An upper limit to the strain at which scission must occur is given by the minimal path lengths of the network. For a site on the bottom wall to which the network is bonded, there are many paths through the polymer network to the top wall. The shortest path is the minimal path P for that site on the bottom wall. For the complete system there is a set of minimal paths, one for each bonding site at the bottom wall. The strain at which the strands in a minimal path are taut, but the bonds are not stretched is given by the relation

$$\epsilon_P = (P - L_z)/L_z \tag{5}$$

where L_z is the unstrained separation distance between the walls. For $\epsilon > \epsilon_P$, some bond within the minimal path must stretch. Using Dijkstra's method,[18] P has been calculated for all bonding sites on the bottom wall. For the system in Figure 1 the shortest minimal path has $\epsilon_P = 0.54$, which is slightly smaller than the first broken bond indicated by the points in the figure. Additional strain is required to stretch bonds to the breaking point. The simulations show that $(P_{av} - L_z)/L_z$ is a good estimate of the failure strain, where P_{av} is the average minimal path over the whole system. For the system in Figure 1 the average value corresponds to $\epsilon_P = 0.97$, which is where the peak stress occurs.

The apparent large failure strain is now understood in terms of the physical constraints on the network connectivity. Bond breaking does not occur until the minimal paths in the network are taut. The strain to make the minimal paths taut is typically about 1, since the typical conformation of a minimal path at $\epsilon = 0$ is a zigzag path as one would expect. Bonds could break at small ϵ if there were an additional constraint operating on a segment of the minimal paths. The fact that the failure strain corresponds to the minimal path strain shows that there are no additional constraints. However, as the number of interfacial bonds is reduced, constraints are effectively transferred from the disallowed bonds to the remaining bonds. This effectively increases the constraints, and the failure strains are smaller than the minimal path strain. These results will be presented in sections IIIE and IIIF.

C. Stress Magnitude. The number of bonds across the interface is an important quantity affecting interfacial fracture. The ideal stress to fracture the interfacial bonds is directly proportional to the number of interfacial bonds per area, N_b.

$$\sigma_{id} = N_b F_b / A \tag{6}$$

where F_b is the force to break a single bond and A is the area of the interface. For systems 2−4 where $N_b \simeq 200$, $F_b = 156.7u_0/d$, and $A = 1928d^2$, $\sigma_{id} = 16.3u_0/d^3$. This ideal value never occurs in the simulations, because the bonds are broken sequentially, not simultaneously (Figure 1). Thus, at any given instant the contribution to the total stress by bond breakage is a fraction of the ideal value. The actual failure stress in Figure 1 is $\sigma_f = 6.2u_0/d^3 = \sigma_{id}/2.6$.

One means to calibrate the simulations is through comparison to measurements on self-assembled monolayers (SAMs). In addition, some fundamental aspects concerning the relative importance of van der Waals and chemical bonds at the interface are revealed. A SAM can be coated onto an atomic force microscope tip, and the force to separate two SAMs can be measured. In this manner molecular scale forces are measured which should correspond to the stresses measured in the simulations. Thomas et al.[19] have measured methyl-terminated alkylsiloxane SAMs as well as COOH:NH_2-terminated SAMs. These two classes of interactions correspond to those involved in bonding of epoxies to silicon oxide surfaces. These experiments measure the pull-off force for a spherical tip of radius, R. To compare to the simulations, the sphere−plane stress needs to be converted to a plane−plane stress. For two surfaces interacting via a LJ potential, the repulsive core can be neglected. Writing the attractive part as $u(r) = -\alpha/r^6$, then it can be shown[20] that the pull-off force between a sphere and a plane is

$$F_{sp} = \frac{\pi^2 \rho^2 \alpha R}{6D^2} \tag{7}$$

where ρ is the number density for both bodies and D is the separation distance. Between two planes the pull-off force per area or stress is

$$\sigma_{pp} = \frac{\pi \rho^2 \alpha}{6D^3} = \frac{F_{sp}}{R} \frac{1}{\pi D} \tag{8}$$

The experimental value for methyl-terminated SAMs is $F_{sp}/R = 0.4 \pm 0.2$ N/m.[19] Taking D as 4 Å, the typical LJ diameter for methyl groups, we obtain $\sigma_{pp} = 320 \pm 160$ MPa. For the acid−base measurements, $F_{sp}/R = 4.3 \pm 0.2$ N/m, which gives $\sigma_{pp} = 3400 \pm 320$ MPa. However, the acid−base interaction has a different potential than the LJ potential. If we use the traditional JKR calculation,[20] we obtain 3100 ± 290 MPa. These two numbers are within the experimental uncertainty so that either number will satisfy the purposes of this discussion. The chemically bonded surfaces require a stress about 10 times larger than the van der Waals bonded surfaces. While measuring the stress at a crack tip is not directly possible, estimates of crack tip stresses for a chemically bonded interface are an order of magnitude lower than the 3.4 GPa. This presents an apparent paradox concerning how bonded interfaces fail at much lower stresses.

The paradox is resolved by recognizing that the number of bonds at the interface for an epoxy adhesive is much smaller than for SAMs. The area per chain for the alkylsiloxane SAMs is about 25 Å^2. The area per cross-linker molecule is calculated using the bulk epoxy density, 1.13 g/cm^3 for the epoxy used in experiments at Sandia.[4,16,21] For a slab with thickness 8 Å near a flat silicon oxide surface, the area per cross-linker is 920 Å^2. For the 6-fold functional cross-linker at the interface assuming on average that three bonds are within the network and three bonds attach to the surface, then the area per interfacial bond is 310 Å^2. Thus, the area per bond in the epoxies is 12 times smaller than in the SAMs. This lowers the ideal fracture stress from 3400 to 280 MPa. However, with the small contact area of a force microscope the bonds between two SAMs break almost simultaneously. In an epoxy, the bonds break successively; i.e., a crack propagates. The present simulations find that this reduces the failure stress by a factor of $\sigma_{id}/\sigma_f = 2.6$. Using this number, the expected local failure stress for epoxies on a silicon oxide surface under tensile strain is about 110 MPa. There are some uncertainties in this number. It is not likely that the cross-linker can make three bonds to the surface. Once one bond is made, the other bonds are restricted to occur in a small area about the first bond. On the other hand, the density at the surface is larger than in the bulk, and this could compensate for the decreased bonding. Thus, including these uncertainties, the true number is not going to be far from 100 MPa. Finally, for epoxies not chemically bonded to a surface, but attached only by van der Waals interactions (i.e., epoxies on a SAM-coated surface to prevent chemical bonding), the failure

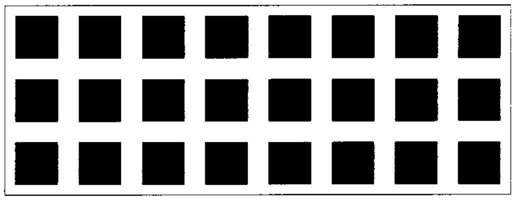

Figure 2. Checkerboard pattern used to create debond areas of varying size is schematically shown. The black squares represent the debond regions. The size of the squares determines the fraction of debond area.

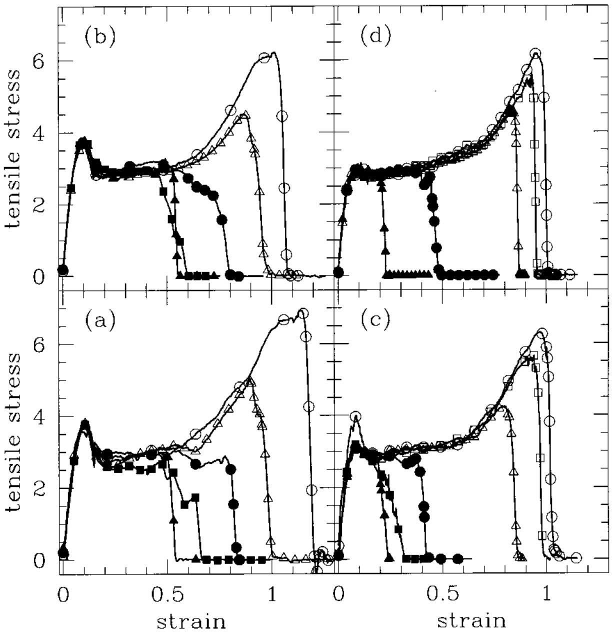

Figure 3. Tensile stress−strain curves for systems 1 (a), 2 (b), 3 (c), and 4 (d). The points represent different bondable area fraction C at the bottom surface: 0% (solid triangle), 10% (solid square), 25% (solid circle), 50%, (open triangle), 75% (open square), 100% (open circle). Stress is in LJ units.

stress is 120 MPa, where the same 2.6 factor has been used. Thus, the contribution to the failure tensile stress due to chemical bonds and the contribution due to van der Waals interactions are comparable. It is important to note that even the van der Waals stress is larger than the bulk epoxy yield stress, which is about 50 MPa, implying that yielding must occur near the crack.

The SAM systems can easily be simulated using the bead−spring system. To each of the top surface beads, a two-bead SAM chain is bonded. Two such model SAM-coated surfaces are created. The stress to separate is calculated just as in the model network systems. The methyl-terminated experiments correspond to simulated SAMs which interact only through the LJ potential, i.e., no bonds connecting the SAMs. In this case, the failure stress is 5.7 u_0/d^3. This implies that $u_0/d^3 = 320/5.7 = 56$ MPa. By bonding each of the two SAM chains opposite each other, the chemically bonded case is treated. In this case, the failure stress is 112 u_0/d^3. This gives a mapping of $u_0/d^3 = 3400/112 = 30$ MPa. Since the model is coarse-grained, and the experimental uncertainty for the van der Waals number is 50%, the two maps are identical. An average value of $u_0/d^3 = 43$ MPa gives the best approximation.

The failure stress of the bead−spring network is 6.2 u_0/d^3. This value is almost equal to the nonbonded SAM failure stress of 5.7 u_0/d^3. This is in good agreement with the calculation from the experimental SAM data which indicated that the epoxy failure stress is about equal to the methyl-terminated SAM failure stress.

D. Variation of Surface Bond Density. Even though the actual value of the fracture stress is not equal to the ideal value, the failure stress may still scale with N_b. To investigate the scaling, the dependence on N_b was examined in a controlled manner by forbidding bonds to occur on a fraction of the wall surface. Experimentally, this is done by coating the surface with SAMs which prevent chemical bonding.[6,7] In the simulations, the bonding reaction is simply forbidden in a chosen region on the wall (Figure 2). The fractional area of the wall surface allowed to bond is denoted by C. The fractional number of bonds at coverage C with respect to full coverage is defined as $n_C = N_b(C)/N_b(C{=}1)$. Because cross-linkers above the edge of a nonbond wall region can move a little and bond to an open site, n_C tends to be slightly larger than C. The ideal fracture stress at coverage C is then

$$\sigma_{id}(C) = N_b(C)F_b/A = n_C\sigma_{id}(C{=}1) \qquad (9)$$

Similar to experimental studies[7] and to get a good statistical representation, a set of rectangles on a grid (Figure 2) demarcate the nonbonding region. In the simulations an 8 × 3 grid was used. Experimentally, such grids coated with SAMs to prevent bonding can be formed lithographically. However, in comparison with such experiments, the simulation nonbonding regions are much smaller, at most 10 nm on a side. Domain sizes of this order may be possible experimentally by applying submonolayer coverages of SAMs at low temperature,[7] although the controlled geometry is lost.

E. Tensile Data. Figure 3 shows the tensile stress−strain curves for systems 1−4 at various C. The shape of the stress−strain curves is similar for all the systems. The molecular deformations for $C = 1$ corresponding to the various stress−strain regimes were described in section III.A. All the systems fail interfacially as discussed above. The variation with system size and bondable area fraction C will now be described.

The $C = 1$ stress−strain curve is a master curve for the lower coverage data. At $C < 1$ the stress−strain curve follows that for $C = 1$ until the failure stress is reached at which point the stress drops to zero. In the tensile mode, this yields two regimes of failure as a function of coverage. For low coverages ($C \leq 0.25$) failure occurs without any secondary rise in the stress due to bond stretching. In this regime, the failure stress is primarily determined by the LJ interactions. At high coverages ($C \geq 0.5$), bond stretching makes a significant contribution.

Figure 3 shows that the failure stress, σ_f, does not vary significantly with system size. Also, at a given C, the shape of the curve is independent of size. In the smaller systems 1 and 2, and for $C = 1$ in system 3, the yield stress is about $4u_0/d^3$. Otherwise for systems 3 and 4, the yield stress is 3 u_0/d^3 with a much less pronounced peak. On the other hand, the failure strain, ϵ_f, does depend on the system size. Consider systems 2 and 4 at $C = 0$. For system 2 ($L_z = 20$), $\epsilon_f = 0.54$, but for system 4 ($L_z = 77$), $\epsilon_f = 0.20$. For the large system, this ϵ_f corresponds to the system failing just after the system has reached the yield stress. This is what one expects for surfaces interacting only through LJ interactions.

F. Shear Data. Figure 4 shows the stress−strain curves for systems 1−4 fractured in shear. The yield

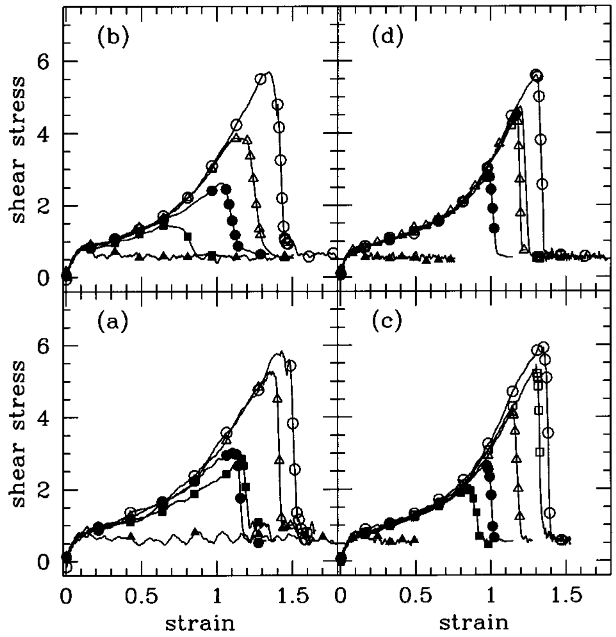

Figure 4. Shear simulation data. Points are the same as in Figure 3.

stress in this case is determined by the $C = 0$ curve which gives $\sigma_y = 0.8u_0/d^3$ independent of the system size. This stress corresponds to the friction force necessary to slide two surfaces with LJ interactions over each other. The friction stress is well-known to be less than the tensile separation stress, since the sliding particles need not fully separate.[22,23] For nonzero bond coverage and strains below the failure strain, the stress rises monotonically with increasing strain. As in the tensile mode, the $C = 1$ stress−strain curve is a master curve. The $0 < C < 1$ curves follow this master curve until failure at which point the stress drops to the yield stress value or sliding friction value.

Comparing Figures 3 and 4 shows that the failure stress in the shear mode at $C = 1$ is the same as in the tensile mode. The failure is also interfacial. Thus, the interfacial strength is the same in either mode. This is not surprising at $C = 1$ where the bond forces dominate in determining the interfacial failure stress. The failure stresses with decreasing C are identical for the two modes until the LJ interactions dominate at low C in the tensile mode.

In contrast to the tensile mode, there is no plateau regime in the shear stress−strain curves. Since yielding in shear mode only involves sliding particles over each other, the particles are not separated at the yield strain as in the tensile mode. In the shear mode, the volume is conserved, and the stress to deform the whole network increases monotonically beyond the yield strain.

In the shear mode, the deformation sequence is the same as the tensile mode, but the strains are larger due to geometric factors. As shown earlier, the failure strain is related to the strain necessary to make taut the minimal paths in the network from the bottom surface to the top surface. This requires a larger strain for the shear mode than for the tensile mode due to geometric effects. For an initial wall separation of $L_z(0)$ and the same strain, the separation distance between two points on the top and bottom walls with same (x, y) positions is $(1 + \epsilon)L_z(0)$ for tensile mode and $\sqrt{1+\epsilon^2}L_z(0)$ for shear mode. For example, at $\epsilon = 1$, the separation distance in tensile mode is $2L_z(0)$, but in shear mode, the separation is only $\sqrt{2}L_z(0)$. Thus, to stretch the minimal paths the same length, the shear simulations must go to larger strains.

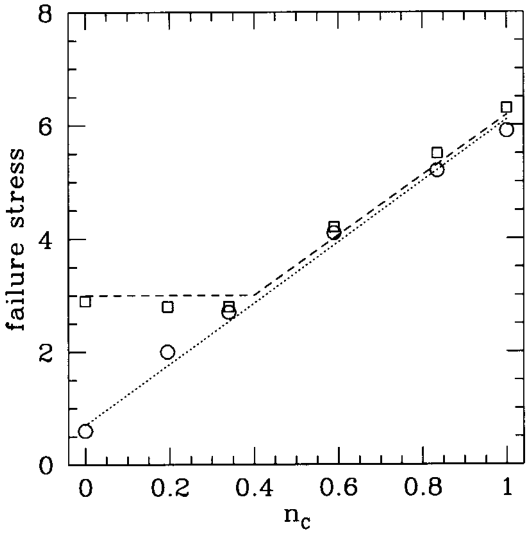

Figure 5. Failure stress in tensile (squares) and shear (circles) simulations as a function of the fractional number of interfacial bonds. Stress is in LJ units.

As in the tensile mode, the failure strain decreases with system size. At $C = 0.25$ for system 2, $\epsilon_f = 1.5$, but for system 4 $\epsilon_f = 1.0$. For the shear mode, the failure stress predominantly has just one regime. For systems 3 and 4, a straight line could be fit through the (ϵ_f, σ_f) points. This implies a linear relation between σ_f and ϵ_f which will be shown in section IV.A.

IV. Discussion

A. Failure Stress. While the magnitude of the failure stress is not equal to the ideal fracture stress, the failure stress still scales as the ideal function. Specifically, let N_1 and N_C be the number of interfacial bonds at full coverage ($C = 1$) and partial coverage, C, respectively. Then, if scaling holds, the stress at C is related to the stress at $C = 1$ by

$$\sigma_C \sim \frac{N_C}{N_1}\sigma_1 + \sigma_{\mathrm{vdW}} = n_C\sigma_1 + \sigma_{\mathrm{vdW}} \qquad (10)$$

where σ_{vdW} is the van der Waals (LJ) contribution. The data for the failure stresses (Figure 5) does in fact exhibit a linear dependence for the shear mode over the complete range of C. The linear fit to the shear data is

$$\sigma_C = 5.4n_C + 0.7 \simeq (\sigma_1 - \sigma_0)n_C + \sigma_{\mathrm{vdW}} \qquad (11)$$

where σ_{vdW} is the failure shear stress at $n_C = 0$.

As noted above the tensile data has two regimes. At low n_C (<0.3), the failure stress is equal to the plateau stress. At larger n_C, the linear fit to the data is almost identical to that for the shear data,

$$\sigma_C = 5.3n_C + 0.8u_0/d^3 \qquad (12)$$

This equation can also be written in terms of plateau

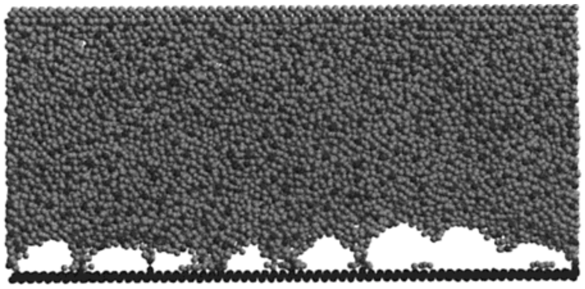

Figure 6. Image[26] of system 2 at $C = 0.1$ under tensile pull at $\epsilon = 0.54$. The pull-off above the nonbonded regions at the bottom surface is clearly exhibited.

stress σ_p, σ_1, and n_C^* the crossover point,

$$\sigma_C = \frac{n_C - n_C^*}{1 - n_C^*}(\sigma_1 - \sigma_p) + \sigma_p, \quad n_C > n_C^* \qquad (13)$$

Here, the van der Waals stress is equal to σ_p. The crossover point is obtained from eq 12 using $\sigma_1 = 6.2u_0/d^3$ and $\sigma_p = 3.0u_0/d^3$, $n_C^* = 0.4$; for $n_C < n_C^*$, $\sigma_C = \sigma_p$. This equation connects σ_p and n_C^* to the y-intercept and slope of eq 12.

B. Failure Strain. For $C = 1$ it was shown earlier that the average minimal path determines the failure strain. For $C < 1$ the average minimal path changes little, but the failure strain decreases substantially. What happens as C decreases from 1, and how does this affect the failure strain? The essential aspect is that the strain becomes inhomogeneous with distinct bulk and interfacial terms.

$$\epsilon = \epsilon_{\text{bulk}} + \epsilon_{\text{int}} \qquad (14)$$

The fewer the bonds at the interface, the larger the difference between ϵ_{bulk} and ϵ_{int}.

Since the walls are pulled at constant velocity, a homogeneous strain would yield a linear displacement profile in both the tensile and shear mode. The mechanism for deviations from the linear profile is exhibited in Figure 6. The figure shows an image of a tensile pull simulation of system 2 at $C = 0.1$ and $\epsilon = 0.54$. Cavities have formed on the bottom surface above the regions which are not chemically bonded to the bottom surface. A few bonds perilously attach the network to the bottom surface. The pull-off of the nonbonded regions occurs at about the same strain as for the completely nonbonded system. In the $C = 0.1$ system at $\epsilon = 0.54$, the stress has already dropped to $1.0u_0/d^3$ from the plateau stress (see Figure 3b). Most of the drop in the stress is due to this pull-off as it occurs before the bonds break. The consequence of the interfacial cavities is that the displacement of monomers near the bottom surface from their initial position is larger than the uniform linear profile.

Displacement profiles for this system have been calculated in the following manner. The displacement of each particle at a given ϵ relative to $\epsilon = 0$ is calculated. Then these particle displacements are averaged in bins parallel to the walls. Figure 7 shows the displacement curves for the system of Figure 6. The first few bins include the wall particles. At the strain of Figure 6 the displacement field shows a large increase at small z near the bottom surface due to the cavity formation. The increase is due to the cavity formation and produces increased stress on the bonds to the surface. The range of the deviation depends on the size of the cavities. The figure shows the progression of this increased interfacial displacement starting from $\epsilon = 0.30$ where the profile is uniform and linear.

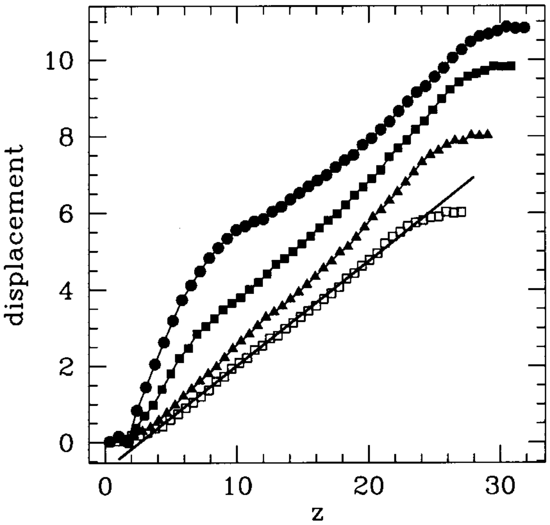

Figure 7. Displacement profile (LJ units) for system 2 at $C = 0.1$ under tensile pull. The data are for the following strains: 0.54 (circle), 0.49 (square), 0.40 (triangle), 0.30 (open square). The circles correspond to the strain of Figure 6. The straight line is a fit to the data for $\epsilon = 0.30$ data excluding the three points on both ends which corresponds to the solid surfaces.

The $C = 0$ and $C = 1$ cases provide boundary values of the failure strain. For $0 < C < 1$, the nonbonded regions will pull off the bottom surface forming cavities at a strain between the failure strains for $C = 0$ and $C = 1$. This will yield an excess in strain or strain localization at the interface. The strain localization causes the segments of the minimal paths within the interfacial region to be excessively stretched. Thus, strain localization is the mechanism by which part of a minimal path can become taut without the whole path becoming taut. Bonds within these segments can and do break well before ϵ_P.

In the shear mode, cavities cannot form at the surface since the volume is conserved. The strain localization still occurs as shown in Figure 8. The deviation from the linear profile occurs in a very narrow region at the surface. In shear mode, the interfacial part of the network in the nonbonded regions can slip over the solid surface. Thus, it does not displace as far as the solid surfaces or the interfacially bonded part of the network. Figure 8 shows the average displacement near the bottom wall tends to be closer to 0 than the wall value. In other words, only the part of the network that must move with the wall does; the rest shears as little as it can. This results in a split between bulk and interfacial strain. Then, just like the inhomogeneity in the tensile strain, this gives the mechanism for a constraint on the minimal path segments which forces them to stretch at $\epsilon < \epsilon_P$.

Figure 9 shows the failure strains as a function of coverage for system 3 (almost identical to system 4) for tensile and shear modes. The linear fit to the shear data is

$$\epsilon_f(n_C) = 0.61n_C + 0.80 \qquad (15)$$

The linear behavior is obeyed for the shear data except at $n_C = 0$ for which no bonds are broken. Thus, the

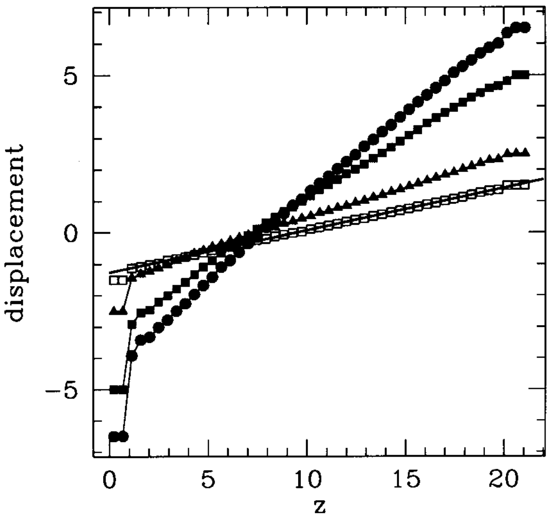

Figure 8. Displacement profile (LJ units) for system 2 at $C = 0.1$ in shear mode. The data are for the following strains: 1.52 (circle), 1.32 (square), 0.99 (triangle), 0.86 (open square). The straight line is a fit to $\epsilon = 0.86$ data excluding the three points on both ends which corresponds to the solid surfaces.

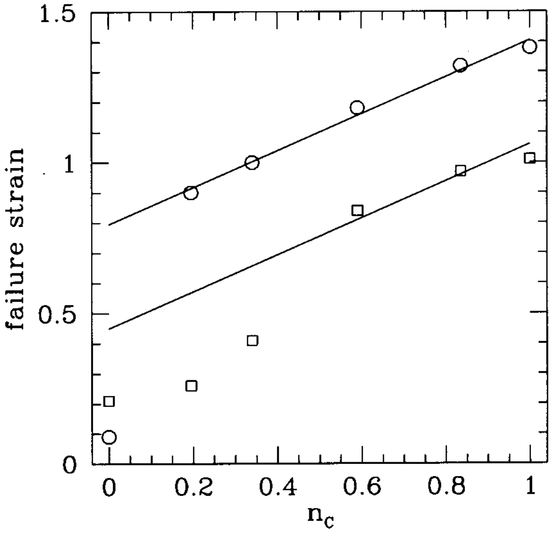

Figure 9. Failure strain in tensile (squares) and shear (circles) simulations as a function of the fractional number of interfacial bonds. A straight line has been fit to the shear data excluding the $n_C = 0$ point, and then the same line but different slope is plotted on the tensile data.

y-intercept is not equal to the $n_C = 0$ failure strain. There is insufficient data to study how the failure strain must tend toward $\epsilon_f(0)$ as $n_C \rightarrow 0$. At small C the number of interfacial bonds is small, yielding poor statistics.

The tensile data in Figure 9 are consistent with the same slope as in eq 15 (albeit for three data points) at $n_C > n_C^*$. As noted earlier, for $n_C < n_C^*$ the failure is dominated in the tensile mode by van der Waals interactions which yields a different behavior. At low n_C, the failure strain deviates from the linear behavior is generally more noisy.

C. Model Modifications. There are a variety of changes to the model that can be made. Some of these would be generic improvements to all systems; others would be to treat specific systems. The system treated here has identical LJ interaction parameters for all species. For nonidentical LJ interactions, there could be preferential adsorption to the surface. This directly effects the relative number of interfacial density of cross-linker and strand beads. The number of interfacial bonds is determined by the interfacial density of cross-linkers. Thus, the interfacial strength is modulated by the relative LJ interactions. Some work has already been done to examine the effect of varying the strength of the polymer−substrate interaction (see also ref 23). The absolute interfacial density is also determined by the wall−bead LJ parameters. The simulations done to date did not reveal any fundamentally different behavior than what has been described above.

The stiffness of the strands affects the failure strains directly. In the present model, the strands are completely flexible, and the extension ratio is large. To make the strands stiffer, a bond bending interaction could be added. In terms of the minimal paths, bond bending constrains the range of accessible angles. With bond bending, the strain at which the minimal path is taut will be smaller as long as the equilibrium angle is less than 180°. Another issue is whether failure could occur at strains even smaller than that corresponding to the maximal extension length. This is equivalent to asking whether the addition of bond bending constraints is sufficient to cause strain inhomogeneities. As discussed above, once inhomogeneity can occur, the failure mechanism becomes more local to the inhomogeneous region. Addressing answer these issues will require the development and addition of an appropriate bond bending potential. The form would have to allow bond breaking which most bond bending potentials do not allow.

The number of bonds from the network to the solid surface is the critical determinate of whether failure is cohesive or adhesive. In the present simulations, the cross-linkers bonding to the surface are allowed to only make a single bond, to have interfacial fracture. Allowing multiple bonds to the surface is underway.[25]

The dependence on the grid size needs to be investigated further primarily for much larger systems. Systems 1 and 2 have different substrate areas. The grid area is consequently different for the same value of C, and the results do not depend on this difference. In addition, a few simulations have been done with the limiting case of a 1 × 1 grid without changing the behavior. This lack of dependence on the grid is expected, given the rather homogeneous structure on the length scales of the simulations. In much larger simulations in which new length scales can enter, the possibility of new effects exists.

V. Conclusions

Initial results have been presented for coarse-grained, bead−spring molecular dynamics simulations of the fracture of highly cross-linked polymer networks bonded to a solid surface. The correspondence between the stress−strain curve and the sequence of molecular deformations has been detailed. For the present model, bonds are not stretched until strains much larger than the yield strain have been reached. The failure strain for a fully bonded surface is equal to the strain necessary to make taut the average minimal path through the network from the bottom solid surface to the top surface. At bond coverages less than full, cavities form above the nonbonded regions. This causes an inhomogeneous strain profile with a bulk and an interfacial term. The inhomogeneous strain is an additional constraint on the network which results in segments of the minimal path near the interface becoming taut (and breaking) well before the full path does. By this mechanism the failure strain is linearly proportional to the number of bonds at the interface. Similarly, the failure stress has a linear dependence on the number of interfacial bonds. The simulations show that sequential bond breaking reduces the fracture stress below the ideal value. In the simulations presented here, failure is always interfacial, because the number of bonds at the interface is smaller than in the bulk.

The above description basically holds for both tensile (mode I) and shear (mode II) deformations. The difference between the two modes occurs because of the strong contribution by van der Waals interactions in the tensile mode. Thus, for weak interfaces which have just a few bonds, the van der Waals interactions determine the failure stress and strain in the tensile mode. In contrast, the van der Waals is always a minor contribution in the shear mode.

Acknowledgment. This work was supported by the DOE under Contract DE-AC04-94AL8500. Sandia is a multiprogram laboratory operated by Sandia Corp., a Lockheed Martin Company, for the DOE.

References and Notes

(1) Brown, H. *Science* **1994**, *263*, 1411.
(2) de Crevoisier, G.; Fabre, P.; Corpart, J.; Leibler, L. *Science* **1999**, *285*, 1246.
(3) Henkee, C.; Kramer, E. *J. Polym. Sci., Polym. Phys. Ed.* **1984**, *22*, 721.
(4) Yim, H.; Kent, M.; McNamara, W.; Ivkov, R.; Satija, S.; Majewski, J. *Macromolecules* **1999**, *32*, 7932.
(5) Reedy, E. D. *Int. J. Solids Struct.* **2000**, *37*, 2429.
(6) Kent, M. S.; Reedy, E. D.; Stevens, M. Molecular-to-Continuum Fracture Analysis of Thermo setting Polymer/Solid Interfaces. Sandia Report SAND No. 2000-0026.
(7) Kent, M. S.; Yim, H.; Matheson, A.; Cogdill, C.; Nelson, G.; Reedy, E. D. *J. Adhes.*, to be published.
(8) Glad, M.; Kramer, E. *J. Mater. Sci.* **1991**, *26*, 2273.
(9) Kinloch, A.; Young, R. *Fracture Behavior of Polymers*; Applied Science Publishers: London, 1983.
(10) Wool, R. *Polymer Interfaces: Structure and Strength*; Hanser: Munich, 1995.
(11) Baljon, A.; Robbins, M. *Science* **1996**, *271*, 482.
(12) Binder, K., Ed. *Monte Carlo and Molecular Dynamics Simulations in Polymer Science*; Oxford: New York, 1995.
(13) Kremer, K.; Grest, G. In *Monte Carlo and Molecular Dynamics Simulations in Polymer Science*; Binder, K., Ed.; Oxford: New York, 1995; Chapter 4, pp 194−271.
(14) de Gennes, P. *Scaling Concepts in Polymer Physics*; Cornell University: Ithaca, NY, 1979.
(15) Kremer, K.; Grest, G. *J. Chem. Phys.* **1990**, *92*, 5057.
(16) Morgan, R.; Kong, F.-M.; Walkup, C. M. *Polymer* **1984**, *25*, 375.
(17) Schneider, J.; Hess, W.; Klein, R. *J. Phys. A* **1985**, *18*, 1221.
(18) Hu, T. *Combinatorial Algorithms*; Addison-Wesley: Reading, 1982.
(19) Thomas, R.; Houston, J.; Crooks, R.; Michalske, T. K. T. *J. Am. Chem. Soc.* **1995**, *117*, 3830.
(20) Israelachvili, J. N. *Intermolecular and Surface Forces*, 2nd ed.; Academic Press: San Diego, 1992.
(21) The epoxy used in the Sandia experiments (ref 4) uses EPON 828 resin and Jeffamine T-403 cross-linker.
(22) Thompson, P. A.; Robbins, M. O. *Phys. Rev. A* **1990**, *41*, 6830.
(23) Yoshizawa, H.; McGuiggan, P.; Israelachvili, J. *Science* **1993**, *259*, 1305.
(24) Gersappe, D.; Robbins, M. O. *Europhys. Lett.* **1999**, *48*, 150.
(25) Stevens, M. Manipulating polymer connectivity to control interfacial fracture, 2000. Sandia Report SAND99-2175J.
(26) Merritt, E.; Bacon, D. *Methods Enzymol.* **1997**, *277*, 505.

MA000553U